Ab Initio G3-type/Statistical Theory Study of the Formation of Indene in Combustion Flames. I. Pathways Involving Benzene and Phenyl Radical†

V. V. Kislov‡ and A. M. Mebel*

Department of Chemistry and Biochemistry, Florida International University, Miami, Florida 33199

Received: October 30, 2006; In Final Form: December 19, 2006

Ab initio G3(MP2,CC)//B3LYP calculations of the potential energy surface (PES) for the formation of indene involving hydrocarbon species abundant in combustion, including benzene, phenyl, propargyl, and methyl radicals, and acetylene, have been performed to investigate the build-up of an additional cyclopenta moiety over the existing six-member aromatic ring. They were followed by statistical calculations of high-pressure-limit thermal rate constants in the temperature range of 300−3000 K for all reaction steps utilizing conventional Rice−Ramsperger−Kassel−Marcus (RRKM) and transition-state (TST) theories. The hydrogen abstraction acetylene addition (HACA) type mechanism, which involves the formation of benzyl radical followed by addition of acetylene, is shown to have low barriers (12−16 kcal/mol) and to be a viable candidate to account for indene formation in combustion flames, such as the 1,3-butadiene flame, where this mechanism was earlier suggested as the major indene formation route (Granata et al. *Combust. Flame* **2002**, *131*, 273). The mechanism of indene formation involving the addition of propargyl radical to benzene and rearrangements on the C_9H_9 PES is demonstrated to have higher barriers for all reaction steps as compared to an alternative pathway, which starts from the recombination of phenyl and propargyl radicals and then proceeds by activation of the C_9H_8 adducts by H abstraction or elimination followed by five-member ring closure in C_9H_7 and H addition to the 2-indenyl radical. The suggested pathways represent potentially important contributors to the formation of indene in combustion flames, and the computed rate constants can be utilized in kinetic simulations of the reaction mechanisms leading to indene and to higher cyclopentafused polycyclic aromatic hydrocarbons (CP-PAH).

1. Introduction

The formation of polycyclic aromatic hydrocarbons (PAH) containing both five- and six-membered rings (so-called cyclopentafused PAH, CP-PAH) is of particular interest because these compounds have been shown to play an important role in reaction mechanisms governing the mass growth of higher PAH, soot, and fullerenes in combustion flames.[1−8] The simple CP-PAH species including indene, fluorene, acenaphthalene, etc., being abundant in flames, may be involved in further PAH growth by the hydrogen abstraction acetylene addition (HACA)[9] sequence producing nonplanar bowl-shaped structures like corannulene (see Figure 1), which has been considered as a substructure and a possible precursor of fullerenes.[1−3,10,11] Indene represents the simplest CP-PAH molecule built from one five- and one six-membered ring fused together, and it has been thought to be an important precursor of higher PAH, even those containing only six-membered rings (e.g., phenanthrene) in combustion flames.[5−8] Indene along with other CP-PAH has been observed as an abundant product in ethane,[12,13] ethylene,[14] *n*-butane,[5] butadiene,[8] heptane,[15] and benzene[4,16] flames as well as in thermal pyrolysis of cyclopentadiene,[17,18] benzene,[19] anthracene,[20] and pyrene.[21]

In their study of the 1,3-butadiene flame, Granata et al.[8] suggested that indene can be formed in the reaction of benzyl radical with acetylene, followed by a closure of a cyclopenta ring. They suggested that such a HACA-type pathway is the major contributor to indene production; however, no theoretical studies of this mechanism have been reported so far. Also, indenyl radical, together with benzyl, propargyl, and cyclopentadienyl radicals, has been demonstrated to play an important role in subsequent reactions of the PAH growth occurring in combustion of 1,3-butadiene.[8]

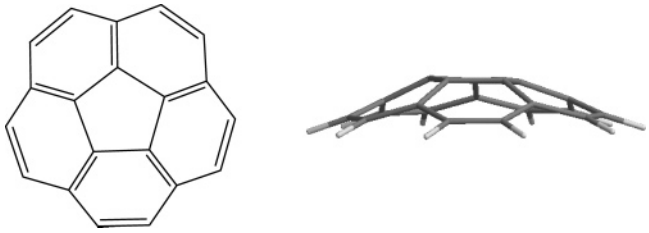

Figure 1. Molecular structure of corranulene, a possible fullerene precursor.

Another mechanism of indene formation involving oxidation of naphthyl radical has been suggested by Marinov and coworkers[5−7] to account for the high yield of phenanthrene in *n*-butane and ethylene flames. According to this mechanism, reaction of molecular oxygen with naphthyl radical produces naphthoxy radical, which then undergoes five-membered ring closure and CO elimination, leading to indenyl radical. In further growth, indenyl may undergo recombination with cyclopentadienyl radical and the product of this reaction eventually rearranges to phenanthrene. The reaction of naphthyl oxidation

† Part of the special issue "James A. Miller Festschrift".

* Author to whom correspondence should be addressed: e-mail mebela@fiu.edu.

‡ Permanent address: Institute of Solution Chemistry of Russian Academy of Sciences, 1 Akademicheskaya St., Ivanovo, 153045 Russia.

10.1021/jp067135x CCC: $37.00
Published on Web 01/30/2007

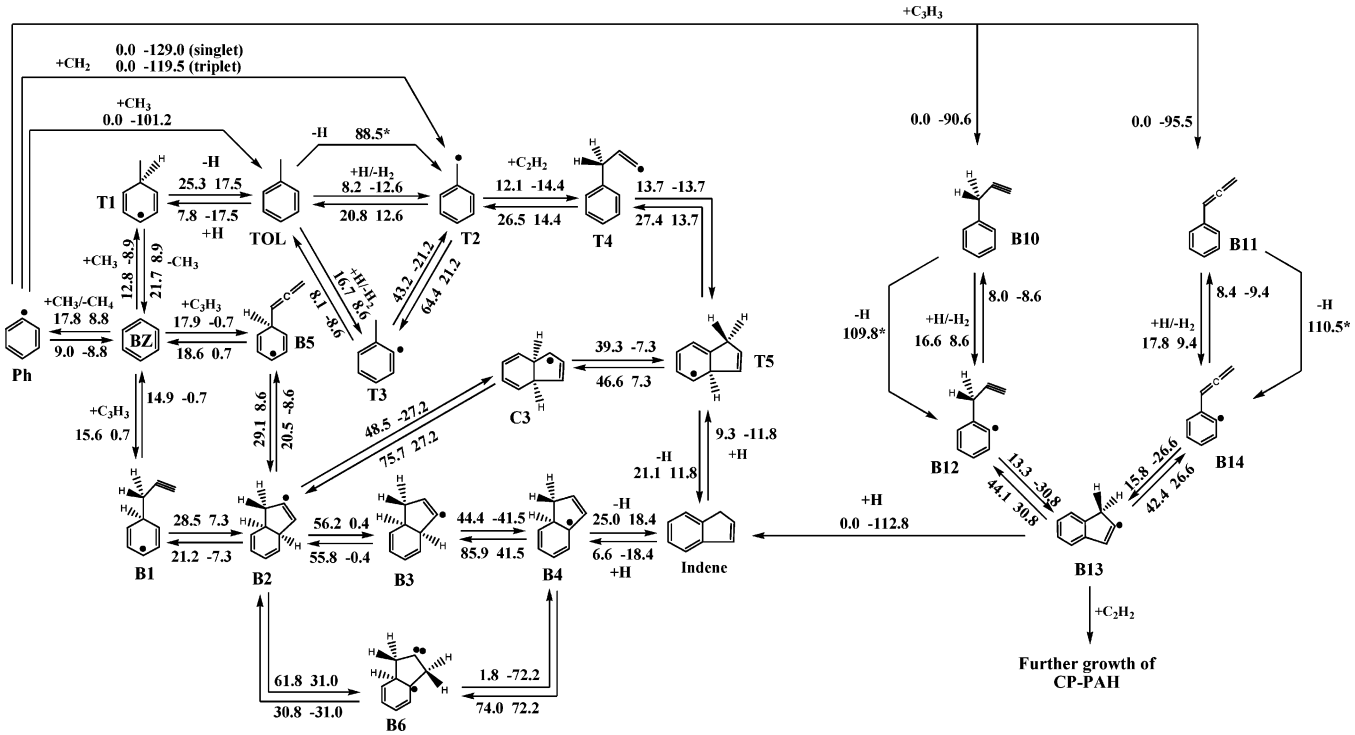

Figure 2. Indene formation pathways involving benzene and phenyl radical. The numbers show G3(MP2,CC)//B3LYP computed barrier heights and heats of reactions at 0 K. Asterisks denote heats of endothermic reactions, which have no exit barriers.

has not been investigated theoretically; however, it is expected to be similar to the reaction of phenyl radical with O_2, which produces another abundant cyclopenta radical, cyclopentadienyl. The latter reaction has been studied thoroughly in the last two decades by various experimental and theoretical methods,[22−30] including recent rather accurate G2M calculations.[30]

Indene, naphthalene and benzene have been found as major reaction products in cyclopentadiene pyrolysis,[17,18] indicating that both cyclopentadienyl and cyclopentadiene represent potential precursors of indene in combustion flames. To explain the high indene yield in cyclopentadiene pyrolysis, Wang et al.[18] suggested the mechanism involving rearrangements of the product of intermolecular addition reaction of cyclopentadienyl radical to a π-bond of cyclopentadiene. According to their density functional theory (DFT) calculations, such a radical−molecular mechanism exhibits reasonably low barriers (12−50 kcal/mol) to account for the indene formation in pyrolysis and in combustion flames as well.

Recently, the mechanisms of intermolecular addition reactions between 1,3-butadiene and phenyl as well as benzene and 1,3-butadien-1-yl radical were investigated at the G2MP2 level, followed by QRRK calculations of reaction rate constants.[31] The computed mechanisms involve reaction pathways leading to indene (after a five-membered ring closure followed by elimination of methyl radical) and naphthalene, indicating that C_4H_6 and C_4H_5 species may also contribute to the formation of indene. However, on the basis of their calculations the authors concluded that production of indene through the C_6H_5 + 1,3-C_4H_6 and C_6H_6 + 1,3-C_4H_5 reaction pathways requires significant activation energies (with high barriers to be overcome), which suggests that indene is most likely formed in flames through alternative reaction channels.

In the present study, we focus on high-level ab initio G3-type calculations of various reaction pathways leading from benzene and phenyl radical to indene, involving the most abundant small hydrocarbon species: propargyl (C_3H_3) and methyl (CH_3) radicals and acetylene (C_2H_2). The ab initio calculations are combined with statistical theory computations of reaction rate constants. The mechanisms studied here only account for the formation of an additional cyclopenta ring over the existing six-membered aromatic cycle. Other potentially important indene formation pathways, which involve abundant cyclopenta species, in particular cyclopentadienyl and fulvene, as well as oxidation of naphthyl radical, will be reported in upcoming publications. Our goal in this work is to reveal the most energetically favorable pathways, to compute their barriers and reaction energies to the best accuracy available for the system size, which can be achieved by employing the G3-type model chemistry approach, and to provide rate constants for future kinetic modeling simulations of CP-PAH formation in combustion systems.

2. Computational Methods

Geometries of all species were optimized by use of the hybrid density functional B3LYP[32] method with the 6-311G** basis set. The same method was used to obtain vibrational frequencies, molecular structural parameters, and zero-point energy (ZPE) corrections and to characterize the stationary points as minima or first-order saddle points. Unscaled vibrational frequencies were used to calculate ZPE corrections and reaction rate constants. In our experience, scaling of B3LYP frequencies does not affect significantly the relative energies of isomers and transition states and RRKM- or VTST-calculated rate constants. Optimized Cartesian coordinates of all local minima and transition-state structures involved in the considered pathways are collected in Table S1 of Supporting Information, along with the unscaled vibrational frequencies, moments of inertia, rotational constants, ZPE corrections, and B3LYP, CCSD(T), MP2, and G3 total energies at 0 K.

To obtain more accurate energies, we applied the G3(MP2,-CC)//B3LYP modification[33] of the original Gaussian 3 (G3) scheme[34] for high-level single-point energy calculations. The final energies at 0 K were obtained by use of the B3LYP

optimized geometries and ZPE corrections according to the formula

$$E_0[\mathrm{G3(MP2,CC)}] = E[\mathrm{CCSD(T)/6\text{-}311G(d,p)}] + \Delta E_{\mathrm{MP2}} + E(\mathrm{ZPE})$$

where $\Delta E_{\mathrm{MP2}} = E[\mathrm{MP2/G3large}] - E[\mathrm{MP2/6\text{-}311G(d,p)}]$ is the basis set correction and E(ZPE) is the zero-point energy. ΔE(SO), a spin−orbit correction, and ΔE(HLC), a higher level correction, from the original G3 scheme were not included in our calculations, as they are not expected to make significant contributions to relative energies. Here and below we denote this G3-type approach used in our computations as G3 for brevity. We applied the Gaussian 98[35] program package to carry out B3LYP and MP2 calculations and the MOLPRO 2002[36] program package to perform calculations of spin-restricted coupled cluster RCCSD(T) energies. The G3-computed barrier heights and heats of reactions (in kilocalories per mole) for all individual reaction steps are shown in Figure 2.

Thermal rate constants at the high-pressure limit were computed by use of conventional RRKM[37−39] and TST[40] theories for unimolecular and bimolecular reactions, respectively. The partition functions were calculated by use of the harmonic oscillator approximation for vibrations and rigid rotor for rotational contributions. The direct count method based on a modified Beyer−Swinehart algorithm[37] was utilized in calculations of the number and densities of states in RRKM computations. Tunneling corrections to the rate constants were calculated with Wigner's formula.[37] All computed rate constants in the 300−3000 K temperature range are collected in Table 1, and the fitted expressions for the rate constants in the form of $k = AT^n \exp(-E/RT)$ are presented in Table S2 of Supporting Information.

3. Results and Discussion

3.1. Indene Formation Pathway Involving Acetylene Addition to Benzyl Radical. The mechanism of acetylene addition to benzyl radical, **T2** → **T4** → **T5** → indene, shown in Figure 2 represents a typical HACA reaction sequence leading to indene through C_2H_2 addition to the radical site of C_7H_7 (**T2**), followed by closure of the cyclopenta ring (**T4** → **T5**), and finally, elimination of an extra hydrogen atom from 9-H-indenyl radical (**T5**). The computed potential energy profile for the $C_7H_7 + C_2H_2$ reaction is depicted in Figure 3. The highest energy transition state on the reaction pathway relative to benzyl radical corresponds to the **T2** → **T4** step and lies only 12.1 kcal/mol above **T2** (see Figure 3). The overall exothermicity of the C_7H_7 (**T2**) + C_2H_2 → C_9H_8 (indene) + H reaction is computed to be 16.3 kcal/mol. According to the experimental study by Granata et al.,[8] benzyl radical was found to be an important PAH precursor in the 1,3-butadiene flame, and in particular, indene is mostly formed in the reaction of benzyl radical with acetylene. Considering that the production of benzyl radicals may be sufficiently high in combustion of other hydrocarbon fuels, this pathway should represent one of the major contributors to the formation of indene in combustion flames.

Benzyl radical (**T2**) itself can be formed from benzene or phenyl radical by several mechanisms. The first one involves a molecular−radical reaction of benzene with methyl radical, **BZ** → **T1**, followed by H-elimination from the **T1** adduct producing toluene, **T1** → **TOL**, and subsequent H-abstraction from the methyl group of toluene, **TOL** → **T2**, to activate a radical site for the further addition of acetylene. The overall reaction for this pathway can be written as $C_6H_6 + CH_3 \rightarrow C_7H_7$ (**T2**) + H_2 and is 4.0 kcal/mol exothermic, with the highest energy transition state for the last H-abstraction step from toluene lying 8.6 kcal/mol above the initial $C_6H_6 + CH_3$ reactants (see the potential energy profile shown in Figure 4). The second mechanism is rather simple and starts from barrierless recombination of phenyl and methyl radicals, producing toluene with an exothermicity of 101.2 kcal/mol, followed by the same H-abstraction from the methyl group of toluene, **TOL** → **T2**. Because this reaction sequence involves three radicals and produces a radical plus a closed-shell molecule, $C_6H_5 + CH_3 + H \rightarrow C_7H_7$ (**T2**) + H_2, it is highly exothermic, by 113.8 kcal/mol overall. Alternatively, the chemically activated toluene molecule formed by the recombination of phenyl and methyl radicals can eliminate a hydrogen atom by cleaving the weakest C−H bond in the methyl group, $C_6H_5 + CH_3 \leftrightarrows C_6H_8$ (TOL) → C_7H_7 (**T2**) + H. This reaction is 12.7 kcal/mol exothermic overall and could be important under low-pressure conditions, where toluene cannot be completely stabilized by collisions. The third mechanism includes barrierless reactions of phenyl radical with singlet or triplet methylene, both of which may be abundant in flames, producing benzyl radical (**T2**). These reactions also demonstrate highly exothermic effects of 129.0 and 119.5 kcal/mol for singlet and triplet CH_2, respectively. It is worth noting that toluene or benzyl radical can be produced from other hydrocarbons abundant in flames, for instance, by the $C_4H_x + C_3H_3$ or $C_5H_x + C_2H_2$ reaction sequences. However, the investigation of these mechanisms is beyond the scope of the present paper.

Intermolecular addition of methyl radical to benzene (**BZ** + CH_3 → **T1**) competes with the abstraction of H-atom by the same methyl radical (**BZ** + CH_3 → **Ph** + CH_4), which produces phenyl + methane. Hence, we included this reaction along with the previously computed G3 barrier and reaction energy[41] in the reaction scheme shown in Figures 2 and 4 to compare the energetics of both reactions. Our results show that the methyl radical addition to benzene exhibits a barrier, which is 5.0 kcal/mol lower than that for the competitive H-abstraction reaction. Also, the former reaction is 8.9 kcal/mol exothermic, whereas the latter is endothermic by nearly the same value of 8.8 kcal/mol. This indicates that the methyl radical addition to benzene is a more energetically favorable channel. A comparison of individual rate constants for the **BZ** + CH_3 → **T1** and **BZ** + CH_3 → **Ph** + CH_4 reactions collected in Table 1 demonstrates that at temperatures up to 1500 K, the addition channel is significantly faster than the competitive abstraction reaction, and at $T = 1500$ K the former reaction is still a factor of 1.6 faster than the latter. However, at higher temperatures the rate constants for both reactions become close and one has to consider the competition between the addition and abstraction channels in kinetic simulations. The analysis of equilibrium constants for the addition and abstraction channels shows that when temperature increases, K_{eq} for the addition reaction decreases (from 250 $\mathrm{cm^3\ mol^{-1}}$ at 500 K to 3.6, 1.4, and 1.1 $\mathrm{cm^3\ mol^{-1}}$ at 1000, 1500, and 2000 K, respectively), whereas K_{eq} of the abstraction reaction rapidly increases (from 5.7×10^{-4} at 500 K to 3.5×10^{-2}, 0.13, and 0.25 at 1000, 1500, and 2000 K, respectively). Therefore, the temperature increase favors the abstraction channel as compared to the addition.

Toluene can be obtained from the **T1** adduct by the elimination of an extra hydrogen atom (**T1** → **TOL**) with a barrier of 25.3 kcal/mol and endothermicity of 17.5 kcal/mol, which are typical for the H-elimination reactions.[41] It should be noted, however, that the H loss from **T1** to produce toluene has to compete with the methyl group loss, **T1** → **BZ** + CH_3,

TABLE 1: RRKM and TST Calculated High-Pressure Limit Thermal Rate Constants[a] for All Studied Reactions Involved in the Formation of Indene in the 300−3000 K Temperature Range

reaction	300 K	500K	600 K	700 K	800 K	900 K	1000 K	1100 K	1200 K	1300 K
BZ + CH_3 → **T1**	3.26×10^{2}	2.26×10^{6}	2.37×10^{7}	1.35×10^{8}	5.25×10^{8}	1.57×10^{9}	3.89×10^{9}	8.37×10^{9}	1.64×10^{10}	2.91×10^{10}
T1 → **BZ** + CH_3	2.34×10^{-3}	8.92×10^{3}	4.22×10^{5}	6.84×10^{6}	5.55×10^{7}	2.87×10^{8}	1.07×10^{9}	3.15×10^{9}	7.76×10^{9}	1.66×10^{10}
BZ + CH_3 → **Ph** + CH_4	5.26×10^{-1}	7.23×10^{4}	1.57×10^{6}	1.48×10^{7}	8.67×10^{7}	3.5×10^{8}	1.11×10^{9}	2.95×10^{9}	6.81×10^{9}	1.41×10^{10}
Ph + CH_4 → **BZ** + CH_3	2.88×10^{5}	1.27×10^{8}	6.81×10^{8}	2.44×10^{9}	6.81×10^{9}	1.57×10^{10}	3.2×10^{10}	5.91×10^{10}	1.01×10^{11}	1.61×10^{11}
T1 → **TOL** + H	2.78×10^{-6}	8.58×10^{1}	6.92×10^{3}	1.65×10^{5}	1.81×10^{6}	1.19×10^{7}	5.41×10^{7}	1.87×10^{8}	5.32×10^{8}	1.29×10^{9}
TOL + H → **T1**	3.65×10^{6}	4.9×10^{8}	1.79×10^{9}	4.63×10^{9}	9.82×10^{9}	1.78×10^{10}	2.94×10^{10}	4.49×10^{10}	6.5×10^{10}	9.03×10^{10}
TOL + H → **T2** + H_2	3.02×10^{6}	5.34×10^{8}	2.14×10^{9}	6.02×10^{9}	1.36×10^{10}	2.66×10^{10}	4.64×10^{10}	7.41×10^{10}	1.12×10^{11}	1.61×10^{11}
T2 + H_2 → **TOL** + H	8.31×10^{-3}	5.59×10^{3}	1.68×10^{5}	2.0×10^{6}	1.33×10^{7}	5.99×10^{7}	2.04×10^{8}	5.75×10^{8}	1.38×10^{9}	2.96×10^{9}
TOL + H → **T3** + H_2	4.57×10^{0}	3.78×10^{5}	7.11×10^{6}	6.08×10^{7}	3.14×10^{8}	1.16×10^{9}	3.38×10^{9}	8.19×10^{9}	1.74×10^{10}	3.36×10^{10}
T3 + H_2 → **TOL** + H	4.29×10^{6}	7.41×10^{8}	2.9×10^{9}	8.13×10^{9}	1.82×10^{10}	3.52×10^{10}	6.14×10^{10}	9.94×10^{10}	1.51×10^{11}	2.19×10^{11}
T3 → **T2**	8.99×10^{-19}	2.12×10^{-6}	2.67×10^{-3}	4.47×10^{-1}	2.11×10^{1}	4.29×10^{2}	4.81×10^{3}	3.52×10^{4}	1.86×10^{5}	7.61×10^{5}
T2 → **T3**	9.07×10^{-34}	3.89×10^{-15}	1.77×10^{-10}	3.78×10^{-7}	1.21×10^{-4}	1.08×10^{-2}	3.96×10^{-1}	7.58×10^{0}	8.95×10^{1}	7.26×10^{2}
T2 + C_2H_2 → **T4**	3.78×10^{2}	2.31×10^{6}	2.3×10^{7}	1.26×10^{8}	4.72×10^{8}	1.37×10^{9}	3.28×10^{9}	6.93×10^{9}	1.31×10^{10}	2.27×10^{10}
T4 → **T2** + C_2H_2	1.10×10^{-6}	1.18×10^{2}	1.34×10^{4}	4.03×10^{5}	5.27×10^{6}	3.98×10^{7}	2.00×10^{8}	7.59×10^{8}	2.30×10^{9}	5.86×10^{9}
T4 → **T5**	6.42×10^{1}	4.85×10^{5}	4.60×10^{6}	2.30×10^{7}	7.69×10^{7}	1.98×10^{8}	4.22×10^{8}	7.86×10^{8}	1.32×10^{9}	2.04×10^{9}
T5 → **T4**	8.75×10^{-8}	1.23×10^{1}	1.40×10^{3}	4.21×10^{4}	5.42×10^{5}	3.97×10^{6}	1.96×10^{7}	7.26×10^{7}	2.16×10^{8}	5.42×10^{8}
T5 → indene + H	3.64×10^{-3}	6.27×10^{3}	2.46×10^{5}	3.51×10^{6}	2.64×10^{7}	1.27×10^{8}	4.59×10^{8}	1.32×10^{9}	3.16×10^{9}	6.71×10^{9}
indene + H → **T5**	1.73×10^{6}	7.23×10^{8}	3.55×10^{9}	1.14×10^{10}	2.85×10^{10}	5.85×10^{10}	1.07×10^{11}	1.77×10^{11}	2.73×10^{11}	3.97×10^{11}
BZ + C_3H_3 → **B1**	1.69×10^{-1}	9.76×10^{3}	1.76×10^{5}	1.48×10^{6}	7.71×10^{6}	2.91×10^{7}	8.73×10^{7}	2.19×10^{8}	4.84×10^{8}	9.64×10^{8}
B1 → **BZ** + C_3H_3	1.69×10^{2}	5.46×10^{6}	7.73×10^{7}	5.22×10^{8}	2.20×10^{9}	6.77×10^{9}	1.68×10^{10}	3.50×10^{10}	6.52×10^{10}	1.10×10^{11}
BZ + C_3H_3 → **B5**	8.07×10^{-3}	2.29×10^{3}	6.14×10^{4}	6.87×10^{5}	4.43×10^{6}	1.97×10^{7}	6.68×10^{7}	1.88×10^{8}	4.56×10^{8}	9.82×10^{8}
B5 → **BZ** + C_3H_3	5.08×10^{-1}	2.06×10^{5}	5.47×10^{6}	5.79×10^{7}	3.42×10^{8}	1.37×10^{9}	4.18×10^{9}	1.04×10^{10}	2.23×10^{10}	4.25×10^{10}
B1 → **B2**	4.13×10^{-9}	5.97×10^{-1}	6.55×10^{1}	1.88×10^{3}	2.33×10^{4}	1.65×10^{5}	7.93×10^{5}	2.86×10^{6}	8.32×10^{6}	2.07×10^{7}
B2 → **B1**	3.22×10^{-3}	7.40×10^{3}	3.09×10^{5}	4.60×10^{6}	3.51×10^{7}	1.73×10^{8}	6.22×10^{8}	1.78×10^{9}	4.26×10^{9}	9.02×10^{9}
B5 → **B2**	9.76×10^{-10}	2.03×10^{-1}	2.43×10^{1}	7.39×10^{2}	9.58×10^{3}	7.04×10^{4}	3.47×10^{5}	1.28×10^{6}	3.79×10^{6}	9.50×10^{6}
B2 → **B5**	1.03×10^{-2}	1.42×10^{4}	5.21×10^{5}	7.03×10^{6}	4.99×10^{7}	2.33×10^{8}	7.99×10^{8}	2.20×10^{9}	5.14×10^{9}	1.05×10^{10}
B2 → **C3**	1.77×10^{-22}	2.26×10^{-8}	8.02×10^{-5}	2.85×10^{-2}	2.37×10^{0}	7.53×10^{1}	1.20×10^{3}	1.18×10^{4}	7.91×10^{4}	4.00×10^{5}
C3 → **B2**	7.67×10^{-43}	7.55×10^{-21}	2.47×10^{-15}	2.19×10^{-11}	2.02×10^{-8}	4.18×10^{-6}	2.98×10^{-4}	9.86×10^{-3}	1.84×10^{-1}	2.19×10^{0}
C3 → **T5**	1.90×10^{-16}	3.83×10^{-5}	2.64×10^{-2}	2.86×10^{0}	9.67×10^{1}	1.53×10^{3}	1.40×10^{4}	8.56×10^{4}	3.91×10^{5}	1.42×10^{6}
T5 → **C3**	2.27×10^{-21}	6.81×10^{-8}	1.64×10^{-4}	4.38×10^{-2}	2.93×10^{0}	7.78×10^{1}	1.09×10^{3}	9.45×10^{3}	5.73×10^{4}	2.64×10^{5}
B2 → **B3**	1.78×10^{-28}	4.83×10^{-12}	6.61×10^{-8}	6.14×10^{-5}	1.05×10^{-2}	5.83×10^{-1}	1.45×10^{1}	2.04×10^{2}	1.85×10^{3}	1.21×10^{4}
B3 → **B2**	3.63×10^{-28}	7.63×10^{-12}	9.82×10^{-8}	8.70×10^{-5}	1.44×10^{-2}	7.79×10^{-1}	1.91×10^{1}	2.64×10^{2}	2.36×10^{3}	1.51×10^{4}
B3 → **B4**	7.33×10^{-20}	5.58×10^{-7}	9.75×10^{-4}	2.07×10^{-1}	1.18×10^{1}	2.77×10^{2}	3.51×10^{3}	2.82×10^{4}	1.61×10^{5}	7.04×10^{5}
B4 → **B3**	6.81×10^{-50}	6.84×10^{-25}	1.27×10^{-18}	3.89×10^{-14}	9.21×10^{-11}	3.90×10^{-8}	5.01×10^{-6}	2.66×10^{-4}	7.36×10^{-3}	1.23×10^{-1}
B4 → indene + H	4.86×10^{-6}	1.29×10^{2}	1.00×10^{4}	2.33×10^{5}	2.53×10^{6}	1.63×10^{7}	7.37×10^{7}	2.53×10^{8}	7.16×10^{8}	1.73×10^{9}
indene + H → **B4**	1.27×10^{8}	9.15×10^{9}	2.87×10^{10}	6.74×10^{10}	1.32×10^{11}	2.25×10^{11}	3.55×10^{11}	5.18×10^{11}	7.23×10^{11}	9.58×10^{11}
B2 → **B6**	1.73×10^{-32}	1.75×10^{-14}	5.93×10^{-10}	1.06×10^{-6}	2.97×10^{-4}	2.42×10^{-2}	8.28×10^{-1}	1.50×10^{1}	1.69×10^{2}	1.33×10^{3}
B6 → **B2**	6.08×10^{-10}	4.23×10^{-1}	6.91×10^{1}	2.68×10^{3}	4.20×10^{4}	3.59×10^{5}	2.00×10^{6}	8.20×10^{6}	2.67×10^{7}	7.25×10^{7}
B6 → **B4**	6.57×10^{11}	1.84×10^{12}	2.38×10^{12}	2.87×10^{12}	3.33×10^{12}	3.71×10^{12}	4.08×10^{12}	4.41×10^{12}	4.70×10^{12}	4.96×10^{12}
B4 → **B6**	1.34×10^{-41}	6.18×10^{-20}	1.69×10^{-14}	1.33×10^{-10}	1.12×10^{-7}	2.14×10^{-5}	1.44×10^{-3}	4.52×10^{-2}	8.02×10^{-1}	9.21×10^{0}

TABLE 1 (Continued)

reaction	300 K	500K	600 K	700 K	800 K	900 K	1000 K	1100 K	1200 K	1300 K
B10 + H → **B12** + H_2	1.67×10^{1}	1.35×10^{6}	2.54×10^{7}	2.15×10^{8}	1.11×10^{9}	4.09×10^{9}	1.19×10^{10}	2.89×10^{10}	6.14×10^{10}	1.18×10^{11}
B12 + H_2 → **B10** + H	5.23×10^{6}	8.49×10^{8}	3.29×10^{9}	9.09×10^{9}	2.03×10^{10}	3.9×10^{10}	6.81×10^{10}	1.1×10^{11}	1.66×10^{11}	2.41×10^{11}
B12 → **B13**	8.59×10^{1}	5.70×10^{5}	5.19×10^{6}	2.52×10^{7}	8.25×10^{7}	2.07×10^{8}	4.37×10^{8}	8.04×10^{8}	1.33×10^{9}	2.05×10^{9}
B13 → **B12**	1.18×10^{-19}	1.67×10^{-6}	3.50×10^{-3}	8.43×10^{-1}	5.19×10^{1}	1.29×10^{3}	1.69×10^{4}	1.40×10^{5}	8.09×10^{5}	3.59×10^{6}
B11 + H → **B14** + H_2	2.58×10^{0}	4.62×10^{5}	1.06×10^{7}	1.04×10^{8}	5.97×10^{8}	2.38×10^{9}	7.41×10^{9}	1.91×10^{10}	4.25×10^{10}	8.43×10^{10}
B14 + H_2 → **B11** + H	3.3×10^{6}	6.93×10^{8}	2.85×10^{9}	8.25×10^{9}	1.92×10^{10}	3.76×10^{10}	6.68×10^{10}	1.1×10^{11}	1.67×10^{11}	2.47×10^{11}
B14 → **B13**	3.83×10^{0}	1.40×10^{5}	1.94×10^{6}	1.27×10^{7}	5.27×10^{7}	1.59×10^{8}	3.84×10^{8}	7.94×10^{8}	1.45×10^{9}	2.43×10^{9}
B13 → **B14**	1.69×10^{-18}	7.22×10^{-6}	1.11×10^{-2}	2.15×10^{0}	1.13×10^{2}	2.47×10^{3}	2.94×10^{4}	2.24×10^{5}	1.21×10^{6}	5.10×10^{6}

reaction	1400 K	1500 K	1700 K	1900 K	2000 K	2200 K	2400 K	2600 K	2800 K	3000 K
BZ + CH_3 → **T1**	4.87×10^{10}	7.77×10^{10}	1.7×10^{11}	3.32×10^{11}	4.45×10^{11}	7.53×10^{11}	1.2×10^{12}	1.81×10^{12}	2.62×10^{12}	3.66×10^{12}
T1 → **BZ** + CH_3	3.21×10^{10}	5.69×10^{10}	1.46×10^{11}	3.07×10^{11}	4.20×10^{11}	7.24×10^{11}	1.14×10^{12}	1.68×10^{12}	2.33×10^{12}	3.10×10^{12}
BZ + CH_3 → **Ph** + CH_4	2.67×10^{10}	4.74×10^{10}	1.25×10^{11}	2.79×10^{11}	3.98×10^{11}	7.47×10^{11}	1.29×10^{12}	2.08×10^{12}	3.19×10^{12}	4.69×10^{12}
Ph + CH_4 → **BZ** + CH_3	2.49×10^{11}	3.64×10^{11}	7.05×10^{11}	1.25×10^{12}	1.59×10^{12}	2.51×10^{12}	3.74×10^{12}	5.34×10^{12}	7.35×10^{12}	9.82×10^{12}
T1 → **TOL** + H	2.77×10^{9}	5.39×10^{9}	1.63×10^{10}	3.91×10^{10}	5.66×10^{10}	1.08×10^{11}	1.86×10^{11}	2.95×10^{11}	4.36×10^{11}	6.17×10^{11}
TOL + H → **T1**	1.2×10^{11}	1.56×10^{11}	2.44×10^{11}	3.6×10^{11}	4.25×10^{11}	5.84×10^{11}	7.71×10^{11}	9.88×10^{11}	1.24×10^{12}	1.53×10^{12}
TOL + H → **T2** + H_2	2.22×10^{11}	2.94×10^{11}	4.84×10^{11}	7.35×10^{11}	8.79×10^{11}	1.22×10^{12}	1.63×10^{12}	2.11×10^{12}	2.64×10^{12}	3.25×10^{12}
T2 + H_2 → **TOL** + H	5.76×10^{9}	1.04×10^{10}	2.84×10^{10}	6.5×10^{10}	9.39×10^{10}	1.79×10^{11}	3.1×10^{11}	5.1×10^{11}	7.89×10^{11}	1.15×10^{12}
TOL + H → **T3** + H_2	5.93×10^{10}	9.76×10^{10}	2.28×10^{11}	4.56×10^{11}	6.14×10^{11}	1.05×10^{12}	1.65×10^{12}	2.45×10^{12}	3.46×10^{12}	4.74×10^{12}
T3 + H_2 → **TOL** + H	3.07×10^{11}	4.13×10^{11}	6.99×10^{11}	1.1×10^{12}	1.34×10^{12}	1.93×10^{12}	2.67×10^{12}	3.58×10^{12}	4.67×10^{12}	5.89×10^{12}
T3 → **T2**	2.58×10^{6}	7.40×10^{6}	4.23×10^{7}	1.70×10^{8}	3.07×10^{8}	8.51×10^{8}	2.02×10^{9}	4.16×10^{9}	7.76×10^{9}	1.33×10^{10}
T2 → **T3**	4.37×10^{3}	2.09×10^{4}	2.74×10^{5}	2.11×10^{6}	5.05×10^{6}	2.26×10^{7}	7.99×10^{7}	2.31×10^{8}	5.75×10^{8}	1.28×10^{9}
T2 + C_2H_2 → **T4**	3.71×10^{10}	5.71×10^{10}	1.21×10^{11}	2.25×10^{11}	2.97×10^{11}	4.85×10^{11}	7.41×10^{11}	1.09×10^{12}	1.53×10^{12}	2.07×10^{12}
T4 → **T2** + C_2H_2	1.32×10^{10}	2.66×10^{10}	8.46×10^{10}	2.11×10^{11}	3.12×10^{11}	6.11×10^{11}	1.06×10^{12}	1.71×10^{12}	2.57×10^{12}	3.67×10^{12}
T4 → **T5**	2.97×10^{9}	4.14×10^{9}	7.09×10^{9}	1.08×10^{10}	1.30×10^{10}	1.79×10^{10}	2.31×10^{10}	2.89×10^{10}	3.49×10^{10}	4.12×10^{10}
T5 → **T4**	1.19×10^{9}	2.39×10^{9}	7.39×10^{9}	1.80×10^{10}	2.63×10^{10}	5.07×10^{10}	8.73×10^{10}	1.39×10^{11}	2.07×10^{11}	2.91×10^{11}
T5 → indene + H	1.28×10^{10}	2.26×10^{10}	5.73×10^{10}	1.20×10^{11}	1.66×10^{11}	2.87×10^{11}	4.53×10^{11}	6.71×10^{11}	9.41×10^{11}	1.26×10^{12}
indene + H → **T5**	5.55×10^{11}	7.47×10^{11}	1.23×10^{12}	1.87×10^{12}	2.24×10^{12}	3.11×10^{12}	4.13×10^{12}	5.29×10^{12}	6.62×10^{12}	8.07×10^{12}
BZ + C_3H_3 → **B1**	1.76×10^{9}	3.04×10^{9}	7.65×10^{9}	1.65×10^{10}	2.31×10^{10}	4.24×10^{10}	7.17×10^{10}	1.14×10^{11}	1.73×10^{11}	2.53×10^{11}
B1 → **BZ** + C_3H_3	1.73×10^{11}	2.56×10^{11}	4.89×10^{11}	8.16×10^{11}	1.01×10^{12}	1.48×10^{12}	2.01×10^{12}	2.62×10^{12}	3.29×10^{12}	4.01×10^{12}
BZ + C_3H_3 → **B5**	1.92×10^{9}	3.49×10^{9}	9.7×10^{9}	2.25×10^{10}	3.27×10^{10}	6.32×10^{10}	1.13×10^{11}	1.86×10^{11}	2.91×10^{11}	4.38×10^{11}
B5 → **BZ** + C_3H_3	7.41×10^{10}	1.19×10^{11}	2.65×10^{11}	4.96×10^{11}	6.48×10^{11}	1.03×10^{12}	1.50×10^{12}	2.07×10^{12}	2.73×10^{12}	3.48×10^{12}
B1 → **B2**	4.50×10^{7}	8.83×10^{7}	2.68×10^{8}	6.47×10^{8}	9.39×10^{8}	1.79×10^{9}	3.07×10^{9}	4.85×10^{9}	7.17×10^{9}	1.00×10^{10}
B2 → **B1**	1.71×10^{10}	2.99×10^{10}	7.44×10^{10}	1.54×10^{11}	2.09×10^{11}	3.57×10^{11}	5.59×10^{11}	8.14×10^{11}	1.12×10^{12}	1.49×10^{12}
B5 → **B2**	2.09×10^{7}	4.15×10^{7}	1.28×10^{8}	3.14×10^{8}	4.57×10^{8}	8.78×10^{8}	1.51×10^{9}	2.41×10^{9}	3.56×10^{9}	5.03×10^{9}
B2 → **B5**	1.94×10^{10}	3.34×10^{10}	8.06×10^{10}	1.64×10^{11}	2.19×10^{11}	3.67×10^{11}	5.68×10^{11}	8.18×10^{11}	1.11×10^{12}	1.47×10^{12}
B2 → **C3**	1.60×10^{6}	5.35×10^{6}	3.93×10^{7}	1.92×10^{8}	3.75×10^{8}	1.20×10^{9}	3.19×10^{9}	7.29×10^{9}	1.48×10^{10}	2.75×10^{10}
C3 → **B2**	1.84×10^{1}	1.16×10^{2}	2.44×10^{3}	2.70×10^{4}	7.56×10^{4}	4.45×10^{5}	1.95×10^{6}	6.85×10^{6}	2.01×10^{7}	5.10×10^{7}
C3 → **T5**	4.31×10^{6}	1.13×10^{7}	5.54×10^{7}	1.96×10^{8}	3.36×10^{8}	8.58×10^{8}	1.87×10^{9}	3.61×10^{9}	6.37×10^{9}	1.04×10^{10}
T5 → **C3**	9.87×10^{5}	3.12×10^{6}	2.05×10^{7}	9.14×10^{7}	1.74×10^{8}	5.24×10^{8}	1.31×10^{9}	2.87×10^{9}	5.62×10^{9}	1.01×10^{10}

TABLE 1 (Continued)

reaction	1400 K	1500 K	1700 K	1900 K	2000 K	2200 K	2400 K	2600 K	2800 K	3000 K
B2 → **B3**	5.99×10^{4}	2.42×10^{5}	2.41×10^{6}	1.50×10^{7}	3.24×10^{7}	1.24×10^{8}	3.81×10^{8}	9.87×10^{8}	2.22×10^{9}	4.53×10^{9}
B3 → **B2**	7.45×10^{4}	2.99×10^{5}	2.93×10^{6}	1.80×10^{7}	3.88×10^{7}	1.48×10^{8}	4.49×10^{8}	1.16×10^{9}	2.59×10^{9}	5.25×10^{9}
B3 → **B4**	2.52×10^{6}	7.64×10^{6}	4.74×10^{7}	2.02×10^{8}	3.75×10^{8}	1.09×10^{9}	2.68×10^{9}	5.69×10^{9}	1.09×10^{10}	1.93×10^{10}
B4 → **B3**	1.37×10^{0}	1.12×10^{1}	3.54×10^{2}	5.47×10^{3}	1.75×10^{4}	1.31×10^{5}	7.02×10^{5}	2.90×10^{6}	9.80×10^{6}	2.84×10^{7}
B4 → indene + H	3.68×10^{9}	7.15×10^{9}	2.14×10^{10}	5.09×10^{10}	7.38×10^{10}	1.41×10^{11}	2.40×10^{11}	3.80×10^{11}	5.60×10^{11}	7.88×10^{11}
indene + H → **B4**	1.24×10^{12}	1.56×10^{12}	2.32×10^{12}	$3.21\ 0^{12}$	3.72×10^{12}	4.86×10^{12}	6.08×10^{12}	7.47×10^{12}	8.97×10^{12}	1.06×10^{13}
B2 → **B6**	7.72×10^{3}	3.61×10^{4}	4.53×10^{5}	3.39×10^{6}	7.92×10^{6}	3.50×10^{7}	1.21×10^{8}	3.43×10^{8}	8.44×10^{8}	1.85×10^{9}
B6 → **B2**	1.71×10^{8}	3.64×10^{8}	1.24×10^{9}	3.30×10^{9}	4.99×10^{9}	1.03×10^{10}	1.88×10^{10}	3.12×10^{10}	4.84×10^{10}	7.07×10^{10}
B6 → **B4**	5.22×10^{12}	5.46×10^{12}	5.86×10^{12}	6.22×10^{12}	6.36×10^{12}	6.66×10^{12}	6.94×10^{12}	7.15×10^{12}	7.34×10^{12}	7.51×10^{12}
B4 → **B6**	7.49×10^{1}	4.59×10^{2}	9.18×10^{3}	9.85×10^{4}	2.69×10^{5}	1.53×10^{6}	6.61×10^{6}	2.27×10^{7}	6.51×10^{7}	1.63×10^{8}
B10 + H → **B12** + H_2	2.1×10^{11}	3.45×10^{11}	8.07×10^{11}	1.61×10^{12}	2.17×10^{12}	3.67×10^{12}	5.81×10^{12}	8.61×10^{12}	1.22×10^{13}	1.66×10^{13}
B12 + H_2 → **B10** + H	3.35×10^{11}	4.49×10^{11}	7.65×10^{11}	1.19×10^{12}	1.46×10^{12}	2.08×10^{12}	2.88×10^{12}	3.86×10^{12}	5.05×10^{12}	6.38×10^{12}
B12 → **B13**	2.95×10^{9}	4.06×10^{9}	6.92×10^{9}	1.05×10^{10}	1.25×10^{10}	1.70×10^{10}	2.20×10^{10}	2.73×10^{10}	3.29×10^{10}	3.87×10^{10}
B13 → **B12**	1.29×10^{7}	3.91×10^{7}	2.44×10^{8}	1.03×10^{9}	1.91×10^{9}	5.50×10^{9}	1.34×10^{10}	2.80×10^{10}	5.33×10^{10}	9.30×10^{10}
B11 + H → **B14** + H_2	1.55×10^{11}	2.61×10^{11}	6.38×10^{11}	1.33×10^{12}	1.82×10^{12}	3.16×10^{12}	5.11×10^{12}	7.77×10^{12}	1.11×10^{13}	1.54×10^{13}
B14 + H_2 → **B11** + H	3.47×10^{11}	4.7×10^{11}	8.13×10^{11}	1.28×10^{12}	1.57×10^{12}	2.27×10^{12}	3.14×10^{12}	4.24×10^{12}	5.54×10^{12}	7.05×10^{12}
B14 → **B13**	3.77×10^{9}	5.52×10^{9}	1.04×10^{10}	1.70×10^{10}	2.11×10^{10}	3.04×10^{10}	4.13×10^{10}	5.32×10^{10}	6.64×10^{10}	8.05×10^{10}
B13 → **B14**	1.75×10^{7}	5.06×10^{7}	2.95×10^{8}	1.18×10^{9}	2.14×10^{9}	5.94×10^{9}	1.40×10^{10}	2.85×10^{10}	5.29×10^{10}	9.05×10^{10}

[a] Units are per second for unimolecular steps and cubic centimeters per second per mole for bimolecular steps.

and the latter process has a lower barrier (by 3.6 kcal/mol as compared to the former) and higher rate constants in the entire 300−3000 K temperature range (see Table 1). If the **T1** adduct is produced, the further formation of benzyl radical requires elimination of a hydrogen atom from the methyl group of toluene. At combustion conditions, such elimination is most likely to be accomplished by the H-abstraction mechanism through the **TOL** → **T2** reaction. In principle, the competitive **TOL** → **T3** H-abstraction from the aromatic ring of toluene is also possible, and in this case, benzyl radical can be produced from **T3** by migration of a hydrogen atom attached to the methyl group to the ortho carbon atom of the benzene ring (**T3** → **T2**) with a barrier of 43.2 kcal/mol. The H-abstraction from methyl group exhibits a low barrier relative to that for the H-abstraction from the benzene ring of toluene, 8.2 versus 16.7 kcal/mol. The abstraction channel to form benzyl is 12.6 kcal/mol exothermic, whereas the abstraction from benzene ring is 8.6 kcal/mol endothermic. We note that the **TOL** → **T3** H-abstraction reaction from toluene shows almost the same energetics as the respective H-abstraction reaction from benzene studied in our previous paper at the same G3 level.[41] A comparison of bimolecular rate constants for the **TOL** + H → **T2** + H_2 and **TOL** + H → **T3** + H_2 reactions (see Table 1) confirms that the H-abstraction from the CH_3 group of toluene is more favorable than from the aromatic ring. Indeed, the former reaction has rate constants that are factors of 13.7, 3.0, and 1.4 higher than those for the latter at 1000, 1500, and 2000 K, respectively, that is, at the temperatures relevant to combustion. Considering the fact that the **T3** → **T2** hydrogen atom migration requires activation energy as high as 43.2 kcal/mol, resulting in low reaction rates (Table 1, we conclude that the **TOL** → **T3** → **T2** sequence is not likely to be competitive with the **TOL** → **T2** H-abstraction step in the formation of benzyl radical under typical combustion conditions. The **T3** radical may be consumed in subsequent HACA growth by reaction with acetylene, and the products are not relevant to the formation of indene.

After benzyl radical is formed, it can react with acetylene, producing 1-phenyl-2-propenyl radical (**T4**) with a barrier of 12.1 kcal/mol and reaction exothermicity of 14.4 kcal/mol. The computed barrier for the acetylene addition to the CH_2 group of benzyl radical is 2−3 times higher than barriers for C_2H_2 addition to phenyl, naphthyl, styryl, phenylethen-2-yl, and phenyl-2-ethynyl radicals in HACA sequences for the formation of naphthalene, acenaphthalene, and phenanthrene.[41,42] In those cases, the barrier heights for acetylene additions were within 3−6 kcal/mol, and respective reaction exothermicities had values in the range of 30−40 kcal/mol, as compared to 12.1 and 14.4 kcal/mol, respectively, for $C_7H_7 + C_2H_2$. For instance, according to our G3 calculations,[41] the well-studied reaction of phenyl radical with acetylene exhibits a low barrier of 3.5 kcal/mol and reaction exothermicity of 39.2 kcal/mol, whereas the most accurate experimental estimate for the barrier of this reaction is 3.1 kcal/mol.[43] The higher barrier (12.1 kcal/mol) for the **T2** → **T4** acetylene addition reaction results in lower reaction rate constants (1−2 orders of magnitude) in the $T = 1000-2000$ K range.

The subsequent closure of a cyclopenta ring in the **T4** adduct leads to the formation of the indene core in the resulting 9-H-indenyl radical (**T5**). This reaction exhibits a barrier of 13.7 kcal/mol, which is close to the corresponding value of 16.6 kcal/mol obtained at the same level of theory for the five-membered ring closure in 1-vinylnaphthalene.[41] The latter reaction is relevant to the formation of another important CP-PAH, acenaphthalene, and both reactions demonstrate similar reaction

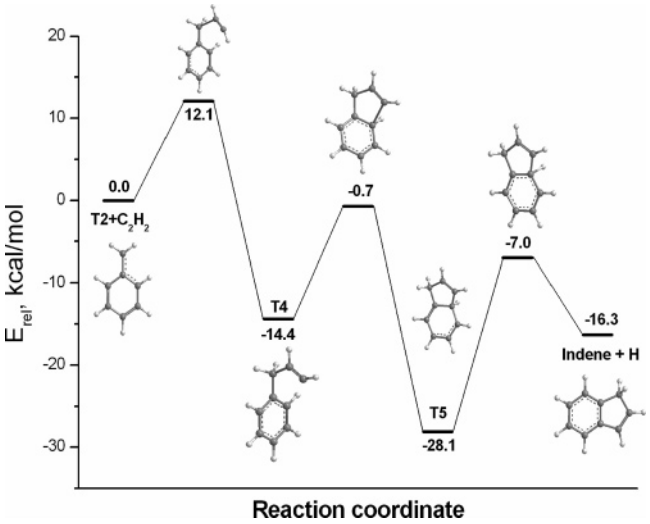

Figure 3. Potential energy diagram for the reaction of benzyl radical **T2** with acetylene calculated at the G3(MP2,CC)//B3LYP level.

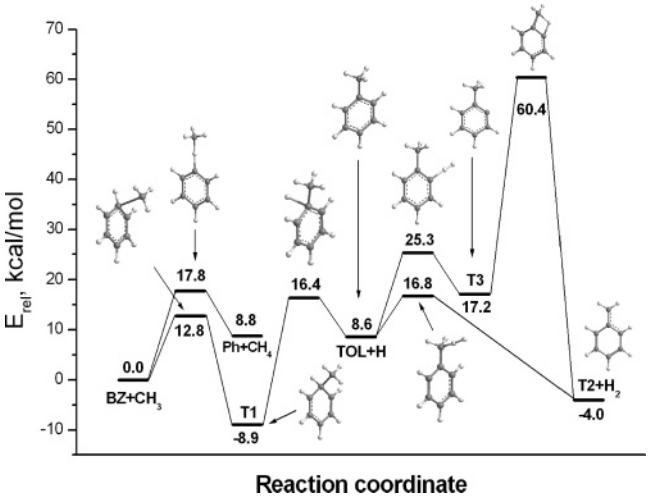

Figure 4. Potential energy diagram for the reaction of benzene **BZ** with methyl radical calculated at the G3(MP2,CC)//B3LYP level.

rate constants.[41] As compared to six-membered ring closure reactions, which normally exhibit barriers of less than 6 kcal/mol,[41] the **T4** → **T5** five-membered ring closure displays a significantly higher barrier of 13.7 kcal/mol, and this value is similar to barrier heights for the other five-membered closure steps (**B12** → **B13** and **B14** → **B13**) considered in the present study. Such a difference is not surprising because a five-membered cycle is more strained than a six-membered aromatic ring and suggests 8−10 kcal/mol difference in strain of five-membered rings in **T5** and **B13** and a six-membered ring in napthyl radical.[41] The final reaction along the considered pathway is elimination of an extra hydrogen atom from 9-H-indenyl radical **T5**, producing indene with a barrier of 21.1 kcal/mol and endothermicity of 11.8 kcal/mol. These values and computed rate constants are in close agreement with those observed for a variety of hydrogen elimination reactions in other HACA pathways.[41,42]

3.2. Indene Formation Pathways Involving Reactions of Benzene and Phenyl with Propargyl Radical. Propargyl radical (C_3H_3) has been shown to be an abundant and resonantly stabilized hydrocarbon radical, which plays an important role in the formation of PAH and soot in combustion flames.[1,44−53] The contribution of the C_3H_3 species to the formation of the first aromatic ring has been studied in detail.[44−47] The detailed

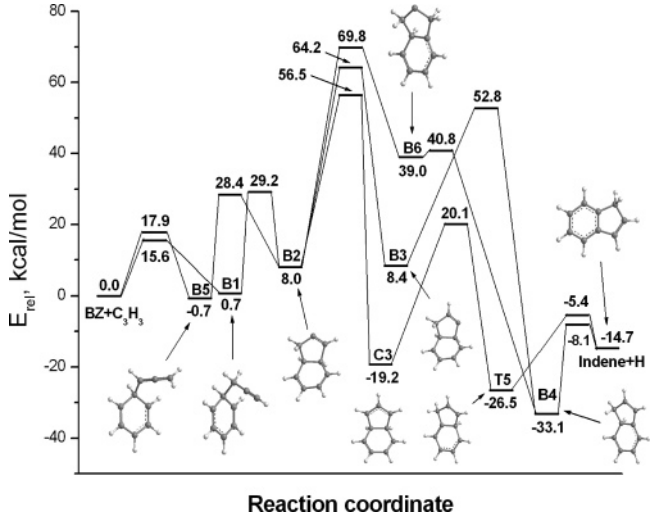

Figure 5. Potential energy diagram for the reaction of benzene **BZ** with propargyl (C_3H_3) radical calculated at the G3(MP2,CC)//B3LYP level.

mechanism involving recombination of two propargyl radicals was first investigated by Miller and Melius and co-workers[48,49] using bond additivity-corrected fourth-order Møller-Plesset perturbation theory (BAC-MP4). The crucial role of C_3H_3 radical in the formation of aromatics has also been generally accepted by the combustion community.[1,51−53] Taking into account the potential importance of C_3H_3 radical, we expect its reactions with benzene and phenyl to be viable sources of indene. Propargyl radical can react with both benzene and phenyl radical. In the case of benzene, one needs to consider a molecular−radical mechanism, that is, intermolecular addition of C_3H_3 to the π-system of benzene, whereas in the latter case, the reaction sequence is initiated by the association of phenyl and propargyl radicals followed by radical activation of a recombination product. Both mechanisms are depicted in Figure 2.

The reaction of propargyl radical with benzene proceeds through several rearrangements on the C_9H_9 potential energy surface (PES), which follow the initial addition step. Figure 5 shows the computed potential energy profile for the C_6H_6 + C_3H_3 reaction. According to our calculations, some of the reaction steps, in particular hydrogen migrations **B2** → **B3**, **B2** → **C3**, **B2** → **B6**, **B3** → **B4**, and **C3** → **T5**, exhibit considerable barriers of 56.2, 48.5, 61.8, 44.4, and 39.3 kcal/mol, respectively. On the other hand, the pathway that starts from barrierless and highly exothermic (∼90−95 kcal/mol) association of phenyl and propargyl radicals subsequently involves activation of the recombination products, either 1-phenyl-2-propyne **B10** or 1-phenyl-1,2-propadiene **B11**, by the H-abstraction mechanism followed by a cyclopenta ring closure, directly producing 2-indenyl radical **B13**. The latter either recombines with a free H radical, leading to indene, or can be involved in further HACA growth of higher CP-PAH. Obviously, the C_6H_5 + C_3H_3 recombination mechanism requires less reaction steps to form indene and these steps exhibit lower barriers (within 14−17 kcal/mol), as compared to the pathway starting from C_3H_3 addition to benzene. However, it costs energy to produce phenyl radical from benzene and the contribution of each pathway will depend on combustion conditions, such as temperature, pressure, fuel type, radical concentrations, etc., and can be clarified in kinetic simulations of particular combustion systems.

The C_3H_3 radical addition to benzene can result in two possible products, **B1** and **B5** radicals, corresponding to the head or tail attack of propargyl toward benzene, respectively, as both

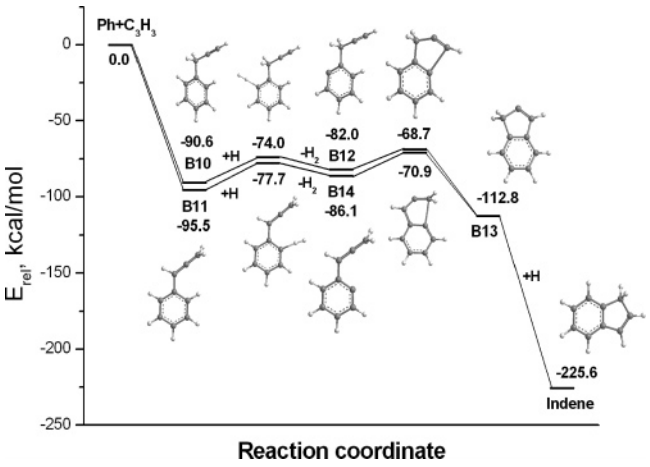

Figure 6. Potential energy diagram for the reaction of phenyl **Ph** and propargyl (C_3H_3) radicals calculated at the G3(MP2,CC)//B3LYP level.

resonance structures of C_3H_3 ($HC{\equiv}C{-}C^{\bullet}H_2$ and $H^{\bullet}C{=}C{=}CH_2$) should be considered. Both reactions demonstrate similar energetics; the barriers are in the 15−18 kcal/mol range and the heats of reactions are close to zero. Calculated rate constants for the **BZ** → **B1** and **BZ** → **B5** addition reactions are similar at the temperatures relevant to combustion (see Table 1). The five-membered ring closures in **B1** and **B5** lead to the same product, 9,10-dihydro-2-indenyl radical **B2**, with barriers of 28.5−29.1 kcal/mol and endothermicities of 7.3−8.6 kcal/mol.

The 8,9-dihydro-2-indenyl radical **B2** may then undergo various H-migration steps, but only three of them, the 1,2-H-shift **B2** → **C3**, the 3,2-H-shift **B2** → **B3**, and the 9,3-H-shift **B2** → **B6**, are relevant to the formation of indene. The **B2** → **B6** H-migration has a barrier of 61.8 kcal/mol and leads to an unstable triradical structure **B6**. This pathway is not competitive. The 1,2-H-shift **B2** → **C3** exhibits a barrier height 7.7 kcal/mol lower than that for the alternative 3,2-H-shift (**B2** → **B3**) leading to 8,9-dihydro-3-indenyl radical. The **B2** → **C3** reaction is exothermic by 27.2 kcal/mol, whereas **B2** → **B3** is nearly thermoneutral. A comparison of rate constants in Table 1 shows that the **B2** → **C3** hydrogen shift is 82, 22, and 12 times faster than the competing **B2** → **B3** reaction at 1000, 1500, and 2000 K, respectively. A comparison of rate constants for the reverse reaction steps also shows that the **B2** → **C3** hydrogen shift is practically irreversible, whereas the forward and reverse rate constants of **B2** ⇆ **B3** are similar. The 8,9-dihydro-1-indenyl radical (**C3**) rearranges to the **T5** radical after the 8,1-H-shift with a barrier of 39.3 kcal/mol; subsequently, elimination of the 9-H-atom from **T5** produces indene. The **B2** → **C3** → **T5** → indene channel is identified as the major indene formation route in the reaction of propargyl radical with benzene at combustion temperatures.

The indene formation mechanism starting from recombination of phenyl and propargyl radicals appears to be more straightforward than C_3H_3 addition to benzene. The entrance C_3H_3 + C_6H_5 recombination step is barrierless, highly exothermic (90−95 kcal/mol, see the potential energy diagram shown in Figure 6), and has two similar paths, head and tail attack of C_3H_3. Two initial adducts are possible, either 1-phenyl-2-propyne (**B10**) or 1-phenyl-1,2-propadiene (**B11**); **B11** is about 5 kcal/mol more stable than **B10**. The recombination reaction leads to the formation of singlet closed-shell species, but the aromatic ring in **B10** and **B11** can be activated by reactions with free radicals abundant in combustion flames. For instance, the **B10** + H → **B12** + H_2 and **B11** + H → **B14** + H_2 hydrogen abstraction steps produce reactive **B12** and **B14** radical species, which then rearrange to 2-indenyl radical **B13** by closing a cyclopenta ring. The computed barriers (16.6 and 17.8 kcal/mol for the **B10** → **B12** and **B11** → **B14** steps, respectively) and heats of reactions (8.6 and 9.4 kcal/mol for the **B10** → **B12** and **B11** → **B14** steps, respectively) are found to be very close to each other, and the calculated values of rate constants for both reactions are also similar (see Table 1). We emphasize that the energetics of the **B10** → **B12** and **B11** → **B14** reactions are very similar to that calculated for the hydrogen abstraction reactions from the aromatic ring in various hydrocarbons, such as benzene, phenylacetylene, vinylacetylene, and naphthalene.[41] For example, the G3 computed barrier height and reaction endothermicity for the H-abstraction from benzene were found to be 17.0 and 8.8 kcal/mol, respectively.[41] Abstraction of hydrogen atoms from positions other than the ortho position in the six-membered rings of **B10** and **B11** is also possible. However, these pathways to 2-indenyl radical **B13** would require H migrations, which usually exhibit high barriers. Under low-pressure and high-temperature conditions, **B12** and **B14** radicals may also be produced by H-elimination from the **B10** and **B11** recombination products; the H-loss reactions are calculated to be endothermic by 109.8 and 110.5 kcal/mol, and the overall C_6H_5 + C_3H_3 → **B10** → **B12** + H and C_6H_5 + C_3H_3 → **B11** → **B14** + H reactions are endothermic by 19.1 and 15.0 kcal/mol, respectively.

In contrast to the rearrangements on the C_9H_9 PES leading to indene from C_3H_3 + benzene, isomerization on the C_9H_7 PES starting from **B12** or **B14** involve only two reaction steps to form indene. The first step is a five-membered ring closure, which produces the indene core in the form of 2-indenyl radical **B13** with the barriers as low as 13.3 and 15.8 kcal/mol for the **B12** → **B13** and **B14** → **B13** steps, respectively. These values are close to the 13.7 kcal/mol barrier height obtained for the similar **T4** → **T5** five-membered ring closure producing 9-H-indenyl radical. The second stage involves recombination of **B13** with an available free H radical, which leads to indene without a barrier and is exothermic by 112.8 kcal/mol. The 2-indenyl radical **B13** may be involved in a further HACA PAH growth by reacting with acetylene, which can lead to higher CP-PAH such as fluorine. This mechanism will be considered in future work.

Summarizing this section, we conclude that the **BZ** + C_3H_3 → **B1/B5** → **B2** → **C3** → **T5** → indene and **Ph** + C_3H_3 → **B10/B11** → **B12/B14** → **B13** → indene sequences can be viewed as potentially important mechanisms of indene formation, involving the reactions of propargyl with benzene and phenyl radical, respectively. The computed rate constants for all considered reaction steps may be utilized in future kinetic simulations aimed to improve the prediction of concentrations of indene and other CP-PAH in combustion flames.

3.3. Remarks on the Accuracy of Calculated Indene Formation Pathways. On the basis of a large number of benchmark calculations, it is well-known that G2 and G3 model chemistry approaches are able to provide chemical accuracy of 1−2 kcal/mol for reaction energies and barrier hieghts.[33,34] Therefore, we can expect similar accuracy for the indene formation network considered in the present study. To test this, we computed reaction energies at 298 K for several crucial reactions relevant to the indene formation mechanisms utilizing experimental heats of formation for benzene, toluene, acetylene, methane, phenyl, methyl, and H radicals from the NIST database.[54] The data for indene and propargyl radical were obtained from different sources, refs 55 and 56, respectively. As seen in Table 2, our G3 calculated values are in good

TABLE 2: G3 Calculated Heats of Chemical Reactions Relevant to the Formation of Indene and Respective Experimental Values[a]

reaction	ΔH(calcd), kcal/mol	ΔH(exp), kcal/mol
$Ph + CH_3 \rightarrow TOL$	−101.2	−104.0
$BZ + CH_3 \rightarrow TOL + H$	8.6	9.4
$BZ + CH_3 \rightarrow Ph + CH_4$	8.8	8.5
$BZ + C_3H_3 \rightarrow$ indene + H	−14.8	−13.3
$BZ + CH_3 + C_2H_2 \rightarrow$ indene + H_2 + H	−20.3	−17.7
$Ph + C_3H_3 + 2H \rightarrow$ indene + H_2	−126.6	−124.5

[a] Experimental values were obtained from available thermodynamic data on heats of formation at 298 K.

agreement with the experimental heats of reactions. Indeed, the observed deviations between experimental and G3 computed results do not exceed 1−3 kcal/mol. Good agreement with the experimental data is also an indication that our B3LYP calculated geometries for all minima and transition states are sufficiently accurate and represent well the structures obtained at the MP2 or CCSD level (MP2 geometries are used in the original G3 scheme). It is known that B3LYP usually performs better than MP2 for open-shell systems, especially for those characterized by high-spin contamination.[57,58] On the other hand, B3LYP is superior to CCSD in terms of the cost of geometry optimization. Although CCSD might produce more accurate geometry than B3LYP, such calculations and especially the calculations of vibrational frequencies are prohibitively expensive for the system size.

4. Conclusions

Chemically accurate ab initio G3-type calculations of PES for the formation of indene starting from benzene and phenyl radical have been performed, followed by statistical calculations of high-pressure limit thermal rate constants. The reaction of benzyl radical with acetylene to produce indene + H is found to be 16.3 kcal/mol exothermic with the highest barrier of 12.1 kcal/mol relative to the reactants for the initial C_2H_2 addition step. The formation of benzyl radical can be accomplished by the addition of methyl radical to benzene followed by a loss of a hydrogen atom, producing toluene, and subsequent H-abstraction from the methyl group of $C_6H_5CH_3$. The $C_6H_6 + CH_3 \rightarrow$ toluene + H reaction is calculated to be 8.6 kcal/mol endothermic and to have a critical barrier of 16.4 kcal/mol. In turn, the toluene + H → benzyl + H_2 abstraction reaction is 12.6 kcal/mol exothermic and exhibits a barrier of 8.2 kcal/mol. The addition of methyl radical to benzene competes with the alternative abstraction channel leading to the formation of $C_6H_5 + CH_4$. The addition reaction is significantly faster than the abstraction at temperatures up to 1500 K, but at higher temperatures both reactions have similar rate constants, and both should be taken into account in kinetic simulations. However, the production of toluene and eventually benzyl radical in the $C_6H_6 + CH_3$ reaction may be hindered because the **BZ** + CH_3 → **T1** equilibrium rapidly shifts toward the reactants with increasing temperature, and also, the reverse **T1** → **BZ** + CH_3 is much faster than the H loss from **T1**, **T1** → **TOL** + H, in the entire 300−3000 K temperature range. Alternatively, benzyl radical can be produced by barrierless recombination of phenyl and methyl radicals to form toluene (exothermic by 101.2 kcal/mol) followed by the H-abstraction (or H-elimination from the CH_3 group, endothermic by 88.5 kcal/mol) and by the reaction of phenyl with methylene, which occurs without a barrier and is exothermic by 119.5 and 129.0 kcal/mol for triplet and singlet CH_2, respectively. In summary, the HACA-type mechanism involving the formation of benzyl radical with subsequent addition of acetylene is shown to have relatively low barriers of 12−16 kcal/mol and is likely to be one of the major indene formation pathways in combustion flames. This conclusion is in agreement with the experimental results measured in 1,3-butadiene flames, where the reaction of benzyl with acetylene was shown to be a dominant source of indene.[8]

The reaction of propargyl radical with benzene leading to indene + H is calculated to be 14.7 kcal/mol exothermic but involves high barriers of at least 56.5 kcal/mol relative to the initial reactants, where the rate-determining step is the intramolecular H shift from the C_9H_9 intermediate **B2** to **C3**. On the other hand, the recombination of phenyl and propargyl radicals leading to the C_9H_8 adducts **B10** and **B11** is barrierless and highly exothermic, by 90.6 and 95.5 kcal/mol, respectively. The **B10** and **B11** intermediates can be activated by H-abstraction through the **B10** + H → **B12** + H_2 and **B11** + H → **B14** + H_2 reactions, endothermic by 8.6 and 9.4 kcal/mol with barriers of 16.6 and 17.8 kcal/mol, respectively. Subsequently, both **B12** and **B14** readily undergo a ring closure to form 2-indenyl radical **B13** with the barriers of 13.3 and 15.8 kcal/mol, respectively, and then 2-indenyl radical can barrierlessly recombine with H, producing indene with exothermicity of 112.8 kcal/mol. The $C_6H_5 + C_3H_3$ mechanism is more favorable energetically than $C_6H_6 + C_3H_3$; however, it requires H-abstraction to activate the initial C_9H_8 recombination products. The importance of the two mechanisms in combustion flames will also be controlled by relative concentrations of the species involved, such as C_6H_6, C_6H_5, H, and C_3H_3.

The suggested pathways represent potentially important contributors to the formation of indene in combustion flames, and the high-pressure limit rate constants generated here can be utilized in future kinetic simulations of various combustion systems.

Acknowledgment. This work was funded by the Chemical Sciences, Geosciences and Biosciences Division, Office of Basic Energy Sciences, Office of Sciences of U.S. Department of Energy (Grant DE-FG02-04ER15570). We thank the reviewers for their valuable comments and suggestions.

Supporting Information Available: Calculated total energies at the B3LYP, CCSD(T), MP2, and G3 levels of theory, zero-point energy corrections, vibrational frequencies, moments of inertia, rotational constants, and optimized Cartesian coordinates of all species involved in the studied mechanisms (Table S1) and fitted rate expressions $k = AT^n \exp(-E/RT)$ for the rate constants of all studied reactions in the 300−3000 K temperature range (Table S2). This material is available free of charge via the Internet at http://pubs.acs.org.

References and Notes

(1) Richter, H.; Howard, J. B. *Prog. Energy Combust. Sci.* **2000**, *26*, 565.

(2) Lafleur, A. L.; Howard, J. B.; Marr, J. A.; Yadav, T. *J. Phys. Chem.* **1993**, *97*, 13539.

(3) Lafleur, A. L.; Howard, J. B.; Taghizadeh, K.; Plummer, E. F.; Scott, L. T.; Necula, A.; Swallow, K. C. *J. Phys. Chem.* **1996**, *100*, 17421.

(4) Righter, H.; Grieco, W. J.; Howard, J. B. *Combust. Flame* **1999**, *119*, 1.

(5) Marinov, N. M.; Pitz, W. J.; Westbrook, C. K.; Vincitore, A. M.; Castaldi, M. J.; Senkan, S. M.; Melius, C. F. *Combust. Flame* **1998**, *114*, 192.

(6) Castaldi, M. J.; Marinov, N. M.; Melius, C. F.; Huang, J.; Senkan, S. M.; Pitz, W. J.; Westbrook, C. K. *Proc. Int. Symp. Combust.* **1996**, *26*, 693.

(7) Marinov, N. M.; Pitz, W. J.; Westbrook, C. K.; Castaldi, M. J.; Senkan, S. M. *Combust. Sci. Technol.* **1996**, *116*, 211.

(8) Granata, S.; Faravelli, T.; Ranzi, E.; Olten, N.; Senkan, S. *Combust. Flame* **2002**, *131*, 273.
(9) Frenklach, M.; Wang, H. *Proc. Combust. Inst.* **1991**, *23*, 1559.
(10) Scott, L. T.; Cheng, P.-C.; Hashemi, M. M.; Bratcher, M. S.; Meyer, D. T.; Warren, H. B. *J. Am. Chem. Soc.* **1997**, *119*, 10963.
(11) Cioslowski, J.; Schimeczek, M.; Piskorz, P.; Moncrieff, D. *J. Am. Chem. Soc.* **1999**, *121*, 3773.
(12) Vincitore, A. M.; Senkan, S. M. *Combust. Flame* **1998**, *114*, 259.
(13) Melton, T. R.; Inal, F.; Senkan, S. M. *Combust. Flame* **2000**, *121*, 671.
(14) Olten, N.; Senkan, S. *Combust. Flame* **1999**, *118*, 500.
(15) Inal, F.; Senkan, S. M. *Combust. Flame* **2002**, *131*, 16.
(16) Marsh, N. D.; Wornat, M. J.; Scott, L. T.; Necula, A.; Lafleur, A. L.; Plummer, E. F. *Polycyclic Aromat. Compd.* **1999**, *13*, 379.
(17) Lu, M.; Mulholland, J. A. *Chemosphere* **2004**, *55*, 605.
(18) Wang, D.; Violi, A.; Kim, D. H.; Mullholland, J. A. *J. Phys. Chem. A* **2006**, *110*, 4719.
(19) Marsh, N. D.; Zhu, D.; Wornat, M. J. *Proc. Combust. Inst.* **1998**, *27*, 1897.
(20) Wornat, M. J.; Vriesendorp, F. J. J.; Lafleur, A. L.; Plummer, E. F.; Necula, A.; Scott, L. T. *Polycyclic Aromat. Compd.* **1999**, *13* (3), 221.
(21) Mukherjee, J.; Sarofim, A. F.; Longwell, J. P. *Combust. Flame.* **1994**, *96*, 191.
(22) Colussi, A. J.; Zabel, F.; Benson, S. W. *Int. J. Chem. Kinet.* **1977**, *9*, 161.
(23) Lin, C.-Y.; Lin, M. C. *J. Phys. Chem.* **1986**, *90*, 425.
(24) (a) Carpenter, B. K. *J. Am. Chem. Soc.* **1993**, *115* (5), 9806. (b) Carpenter, B. K. *J. Phys. Chem.* **1995**, *99*, 9801.
(25) Mebel, A. M.; Lin, M. C. *J. Am. Chem. Soc.* **1994**, *116*, 9577.
(26) Lin, M. C.; Mebel, A. M. *J. Phys. Org. Chem.* **1995**, *8*, 407.
(27) Fadden, M. J.; Barckholtz, C.; Haddad, C. M. *J. Phys. Chem. A* **2000**, *104*, 3004.
(28) Fadden, M. J.; Hadad, C. M. *J. Phys. Chem. A* **2000**, *104*, 8121.
(29) Merle, J. K.; Hadad, C. M. *J. Phys. Chem. A* **2004**, *108*, 8419.
(30) Tokmakov, I. V.; Kim, G. S.; Kislov, V. V.; Mebel, A. M.; Lin, M. C. *J. Phys. Chem. A* **2005**, *109*, 6114.
(31) Fascella, S.; Cavallotti, C.; Rota, R.; Carra S. *J. Phys. Chem. A* **2004**, *108*, 3829.
(32) (a) Becke, A. D. *J. Chem. Phys.* **1992**, *96*, 2155. (b) Becke, A. D. *J. Chem. Phys.* **1992**, *97*, 9173. (c) Becke, A. D. *J. Chem. Phys.* **1993**, *98*, 5648. (d) Lee, C.; Yang, W.; Parr, R. G. *Phys. Rev.* **1988**, *B37*, 785.
(33) (a) Baboul, A. G.; Curtiss, L. A.; Redfern, P. C.; Raghavachari, K. *J. Chem. Phys.* **1999**, *110*, 7650. (b) Curtiss, L. A.; Raghavachari, K.; Redfern, P. C.; Baboul, A. G.; Pople, J. A. *Chem. Phys. Lett.* **1999**, *314*, 101.
(34) Curtiss, L. A.; Raghavachari, K.; Redfern, P. C.; Rassolov, V.; Pople, J. A. *J. Chem. Phys.* **1998**, *109*, 7764.
(35) Frisch, M. J.; Trucks, G. W.; Schlegel, H. B.; Scuseria, G. E.; Robb, M. A.; Cheeseman, J. R.; Zakrzewski, V. G.; Montgomery, J. A.; Stratmann, R. E.; Burant, J. C.; Dapprich, S.; Millam, J. M.; Daniels, R. E.; Kudin, K. N.; Strain, M. C.; Farkas, O.; Tomasi, J.; Barone, V.; Cossi, M.; Cammi, R.; Mennucci, B.; Pomelli, C.; Adamo, C.; Clifford, S.; Ochterski, J.; Petersson, G. A.; Ayala, P. Y.; Cui, Q.; Morokuma, K.; Salvador, P.; Dannenberg, J. J.; Malick, D. K.; Rabuck, A. D.; Raghavachari, K.; Foresman, J. B.; Cioslowski, J.; Ortiz, J. V.; Baboul, A. G.; Stefanov, B. B.; Liu, G.; Liashenko, A.; Piskorz, P.; Komaromi, I.; Gomperts, R.; Martin, R. L.; Fox, D. J.; Keith, T.; Al-Laham, M. A.; Peng, C. Y.; Nanayakkara, A.; Challacombe, M.; Gill, P. M. W.; Johnson, B.; Chen, W.; Wong, M. W.; Andres, J. L.; Gonzalez, C.; M. Head-Gordon, M.; Replogle, E. S.; Pople, J. A. *Gaussian 98*, revision A.11; Gaussian, Inc.: Pittsburgh, PA, 2001.
(36) Amos, R. D.; Bernhardsson, A.; Berning, A.; Celani, P.; Cooper, D. L.; Deegan, M. J. O.; Dobbyn, A. J.; Eckert, F.; Hampel, C.; Hetzer, G.; Knowles, P. J.; Korona, T.; Lindh, R.; Lloyd, A.W.; McNicholas, S. J.; Manby, F. R.; Meyer, W.; Mura, M. E.; Nicklass, A.; Palmieri, P.; Pitzer, R.; Rauhut, G.; Schutz, M.; Schumann, U.; Stoll, H.; Stone, A. J.; Tarroni, R.; Thorsteinsson, T.; Werner, H.-J. MOLPRO, a package of ab initio programs designed by H.-J. Werner and P. J. Knowles, version 2002.1.
(37) Steinfield, J.; Francisco, J.; Hase, W. *Chemical Kinetics and Dynamics*; Prentice-Hall: Englewood Cliffs, NJ, 1989.
(38) Eyring, H.; Lin, S. H.; Lin, S. M. *Basic Chemical Kinetics*; Wiley, New York, 1980.
(39) Robinson, P. J.; Holbrook, K. A. *Unimolecular Reactions*; Wiley, New York, 1972.
(40) Glasstone, S.; Laidler, K. J.; Eyring, H. *The Theory of Rate Processes*; McGraw-Hill: New York, 1941.
(41) Kislov, V. V.; Islamova, N. I.; Kolker, A. M.; Lin, S. H.; Mebel, A. M. *J. Chem. Theory Comput.* **2005**, *1*, 908.
(42) Kislov, V. V.; Mebel, A. M.; Lin, S. H. *J. Phys. Chem. A* **2002**, *106*, 6171.
(43) Yu, T.; Lin, M. C.; Melius, C. F. *Int. J. Chem. Kinet.* **1994**, *26*, 1095.
(44) Hurd, C. D.; Macon, A. R.; Simon, J. I.; Levetan, R. V. *J. Am. Chem. Soc.* **1962**, *84*, 4509.
(45) Wu, C. H.; Kern, R. D. *J. Phys. Chem.* **1987**, *91*, 6291.
(46) Frenklach, M.; Yuan, T.; Ramachandra, M. K. *Energy Fuels* **1988**, *2*, 462.
(47) Hidaka, Y.; Nakamura, T.; Miyauchi, A.; Shiraishi, T.; Kawano, H. *Int. J. Chem. Kinet.* **1989**, *21*, 643.
(48) Miller, J. A.; Melius, C. F. *Combust. Flame*. **1992**, *91*, 21.
(49) Melius, C. F.; Colvin, M. E.; Marinov, N. M.; Pitz, W. J.; Senkan, S. M. *Proc. Int. Symp. Combust.* **1996**, *26*, 685.
(50) Richter, H.; Howard, J. B. *Phys. Chem. Chem. Phys.* **2002**, *4*, 2038.
(51) Miller, J. A. *Faraday Discuss.* **2001**, *119*, 461.
(52) Miller, J. A.; Klippenstein, S. J. *J. Phys. Chem. A* **2003**, *107*, 7783.
(53) Howe, P.-T.; Fahr, A. *J. Phys. Chem. A* **2003**, *107*, 9603.
(54) NIST Chemistry WebBook, http://webbook.nist.gov/chemistry/, NIST Standard Reference Database Number 69, June 2005 release.
(55) *CRC Handbook of Chemistry and Physics*, 87th ed., 2006−2007; CRC Press: Boca Raton, FL, 2006.
(56) Roth, W. R.; Hoff, H.; Horn, C. *Chem. Ber.* **1994**, *127*, 1781.
(57) Mayer, P. M.; Parkinson, C. J.; Smith, D. M.; Radom, L. *J. Chem. Phys.* **1998**, *108*, 604.
(58) Mebel, A. M.; Morokuma, K.; Lin, M. C. *J. Chem. Phys.* **1995**, *103*, 7414.